

Article

Tribology and Micromechanics of Chromium Nitride Based Multilayer Coatings on Soft and Hard Substrates

Juergen M. Lackner ^{1,*}, Wolfgang Waldhauser ¹, Lukasz Major ² and Marcin Kot ³

¹ JOANNEUM RESEARCH Forschungsgesellschaft mbH, Institute of Surface Technologies and Photonics, Functional Surfaces, Leobner Strasse 94, A-8712 Niklasdorf, Austria;
E-Mail: wolfgang.waldhauser@joanneum.at

² Polish Academy of Sciences, Institute of Metallurgy and Materials Sciences, Ul. Reymonta 25, 30-059 Krakow, Poland; E-Mail: l.major@imim.pl

³ AGH University of Science and Technology, Faculty of Mechanical Engineering and Robotics, Laboratory of Tribology and Surface Engineering, A. Mickiewicza Ave. 30, 30-059 Krakow, Poland
E-Mail: kotmarc@imir.agh.edu.pl

* Author to whom correspondence should be addressed; E-Mail: juergen.lackner@joanneum.at;
Tel./Fax: +43-316-8769-2305.

Received: 25 December 2013; in revised form: 24 January 2014 / Accepted: 27 January 2014 /

Published: 12 February 2014

Abstract: The tribological protection of carbon fiber reinforced epoxy composites (CFC) is essential for broadening their use from structural to functional applications, e.g., to linear bearings in mechanical engineering. However, their wear resistance in sliding and rolling contacts is low. This work focusses on the possibility of improving their tribological properties by the application of thin hard multi-layered coatings. Chromium nitride (CrN) single layer and chromium-CrN multilayer coatings of ~4 μm thickness, partly finished with a 1 μm diamond-like carbon (DLC) top layer, were deposited by magnetron sputtering at low temperatures on soft CFC and for comparison of the mechanical behavior on comparatively hard austenitic steel substrates. Structural investigations showed especially that the multilayer coatings possess a very fine grained, columnar microstructure and a very low density of intercolumnar micro-cracks, while the single layer coatings possess a coarse structure. The indentation testing and the analysis of the deformed and fractured cross-sections revealed a tougher behavior with improved plastic deformability of the multilayers in comparison to CrN single layers. However, in wear testing only coatings with DLC top layers significantly improved the tribological material properties of CFC. This is due to the reduced shear forces in sliding on low-friction DLC coatings on the soft

epoxy-based CFC, decreasing the total dynamic stresses during sliding under high loads.

Keywords: carbon fiber composite; magnetron sputtering; multilayer coatings; chromium nitride; diamond-like carbon; microstructure; tribology

1. Introduction

High strength, fiber reinforced polymers like carbon fiber composites (CFC) are state-of-the-art ultra-high strength light-weight construction materials, which are fabricated in highly complex shapes and widely used as structural components in automotive, aerospace, medical technology, and mechanical engineering. Nevertheless, their functional performance in terms of abrasion, sliding, and impact wear resistance is low, limiting their use under higher tribological strains. Additionally, replacing steel components by light-weight CFC of similar mechanical bulk strength often requires an effective surface wear protection.

Besides nowadays in used constructions combining functionally strained metal and ceramic components with CFC, the coating of the polymer composite is seen as a mechanically and economically favorable option for the future. Thick coatings can be obtained from electrochemical and spray technologies, which guarantee high load support but lack in adhesion during overloading due to high stiffness and low plastic deformability for the following substrate deflection [1–3]. Mechanically, this phenomenon is described based on bending stresses [4]: During mechanical loading, brittle ceramic coatings crack under the bending stresses generated by elastic or plastic deformation of the subjacent soft substrate. The thicker such hard ceramic coating on such a deformable substrate are, the higher the bending stress is. Alternatively, thick soft polymer coatings (pure and micro-/nanoparticle strengthened lacquers) possess high elasticity following substrate deflection, but their tribological resistance is not sufficiently high [5].

Thin films of materials combining hardness and wear resistance with high compliance as well as high toughness are future candidates for the tribological protection of functionally-used polymers [6–8]: Single layer hard coatings like chromium nitride (CrN) on CFC substrates, presented by Kääriänen *et al.* [9], do not fulfill the high demands for tribological protection: The problems, stated by the authors, were both the very inhomogeneous and highly rough CFC surface and the need for bridging high to low elasticity from polymer to hard coating. Deposition of dense, continuous coatings with high adhesion to the CFC substrate was impossible. An additional problem, described and detailed by Lackner *et al.* [10], is the very different thermal expansion of composites and hard coatings, leading to stresses, wrinkling and buckling phenomena and finally film delamination. Consequently, the development of coatings for CFC substrates must fulfill all these major demands: (1) Sub-millimeter sized inhomogeneous surface topography and structure require new CFC manufacturing methods for ultra-smooth CFC types. (2) Elasticity and toughness of hard coatings must be based on multilayered structures, which have generally higher resistance to cohesive and adhesive crack propagation compared to single layered coating types [11,12]. (3) Effective temperature control methods during film deposition as well as limited deposition rates are essential to prevent thermal damage (e.g., degradation) of the CFC surface as well as any thermal stress induced effects in thin film growth.

This work focusses on multilayered coating structures on soft, flexible CFC composites substrates in comparison to comparatively hard and stiff austenite steel: While the majority of commercially available state-of-the-art wear resistant coatings consists of one or a couple of single hard layers with high sensitivity to through-thickness fracture [11,12], the placement of softer layers in between hard ones may allow arresting the propagation of cracks at the internal interfaces by energy dissipation and crack deflection [13,14]. The improved toughness of such coatings is furthermore due to the nano-scale shearing of the hard layers on the softer (inter-)layers, preventing the build-up of high-bending stresses [13–15]. Such a material combination can simultaneously increase hardness and reduce the intrinsic growth stresses, which results in markedly improved wear resistance [16,17]. The coating materials in this work, chromium (Cr)/chromium-nitride (CrN) multilayers with diamond-like carbon (DLC, a-C:H) top layers, were manufactured by unbalanced magnetron sputtering at low temperatures to prevent damage of the substrate materials due to mechanical distortion or chemical de-polymerization. To show and discuss the improvements and their physical origins, single layer coating types as well as coating structures without DLC top layers were also investigated. High-resolution transmission electron microscopy (HR-TEM) techniques were finally used to describe the mechanisms of the multilayer deformation and for improving the tribological behavior in contact to Al_2O_3 and AISI 5210 steel counterparts.

2. Experimental Section

2.1. Coating Deposition

Before the deposition started, the CFC (carbon fiber composite with high-modulus carbon fibers in epoxy matrix), and polished austenitic steel substrates (DIN EN 1.4301, AISI 304) were cleaned ultrasonically by ethanol and dried. After mounting on the substrate carousel, the vacuum chamber was pumped down to the start pressure for deposition (2×10^{-3} Pa). Plasma etching by an anode layer ion source (ALS [18]) was applied to remove micrometer sized contaminations and to chemically activate the composite surface in an oxygen atmosphere. Unbalanced magnetron sputtering in an industrially-scaled, 4 rectangular cathode vacuum chamber was chosen to deposit Cr, CrN, and DLC coatings from high purity chromium (99.99%, RHP Technology GmbH, Seibersdorf, Austria) and electrographite carbon targets (99.9%, Schunk Group, Bad Goisern, Austria), respectively. The following coating architectures were developed based on former works [19,20]:

- (1) single layer Cr (3.94 μm thickness);
- (2) Cr-CrN multilayer with totally 16 Cr-CrN bilayers and a modulation ratio CrN:Cr = 2:1 (82 nm Cr + 168 nm CrN) (total thickness 3.99 μm);
- (3) Cr-CrN multilayer with totally 32 Cr-CrN bilayers and a modulation ratio CrN:Cr = 2:1 (42 nm Cr + 84 nm CrN) (total thickness 4.18 μm);
- (4) Cr-CrN multilayer similar to (3), but with a 1 μm thick DLC top coating (thickness 5.16 μm).

Cr as well as DLC deposition occurred in inert argon process gas. For CrN a mixture of Ar and N_2 was used in reactive deposition. A bias voltage of -50 V DC was applied to increase the energy density on CFC substrates. The DC magnetron power was controlled to prevent too high substrate heating exceeding the low thermal stability of the epoxy matrix, degrading above ~ 140 °C. To provide a

homogenous film thickness of the whole coated surface and to simulate industrial batch coating deposition conditions, the substrates were rotated during ALS pre-treatment and coating.

2.2. Coating Characterization

Scanning electron microscopy (SEM, EVO 50, Zeiss, Oberkochen, Germany) was used to study the growth structure on the cross-sections and the surface morphology. Cutting with an ATM Brilliant 221 system was performed up to 2/3 of the sample thickness from the backside, for the sample preparation. Fracturing of the coated CFC substrates occurred manually by tensile loading with pincers. For increasing the conductivity during microscopy imaging, the specimens were evaporated with gold.

The micro- and nanostructure of the coatings were analyzed by the application of transmission electron microscopy (TEM, TECNAI G2 F20 (200 kV FEG), Hillsboro, OR, USA) after focused ion beam based cross-section sample preparation (Quanta 200 3D DualBeam microscope equipped with *in-situ* OmniProbe micro manipulator, gallium ions for milling). Electron diffraction patterns in high resolution mode (HR) were used for structural analyses, while the bright field (BF) technique was applied for imaging of the coating architecture and of the fracture behavior and mechanisms below the spherical indents. Structural investigations were performed on a Bruker AXS D8 Advance diffractometer with CuK α radiation, equipped with a Sol-X detector and a Göbel mirror. The Bragg-Brentano scanning geometry (locked couple) was applied between 20 ° and 80 ° with a step width of 0.02 ° and 1.2 s measurement duration per step, whereby comparative measurements to the coated CFC substrates were performed with coated silicon.

The film thickness on masked steps, as well as the arithmetic roughness (R_a), were measured by stylus profilometry (Dektak 150, Veeco, Santa Barbara, CA, US). The hardness (H) and the elastic modulus (E) of the coatings were obtained from nanoindentation testing with a Vickers indenter on a Fisherscope H100C (Helmut Fischer GmbH, Sindelfingen-Machingen, Germany) device according to DIN EN ISO 14577-1:2002 [21]. The applied maximum load was 50 mN, the loading rate 20 nm s⁻¹ for all measurements, which prevented any high substrate compliance influence on the coating properties (indentation depth <10% of film thickness). The indentation results were analyzed afterwards using the Oliver and Pharr theory [22] in order to get H and E . Cone shaped diamond indenters with 20 μ m tip radius were used for the indentation at 2 N normal force to achieve the desired fracture in the single and multilayer coatings by elastoplastic substrate deflection. Subsequent analysis of the deformation and coating fracture mechanisms was done by TEM and HR-TEM.

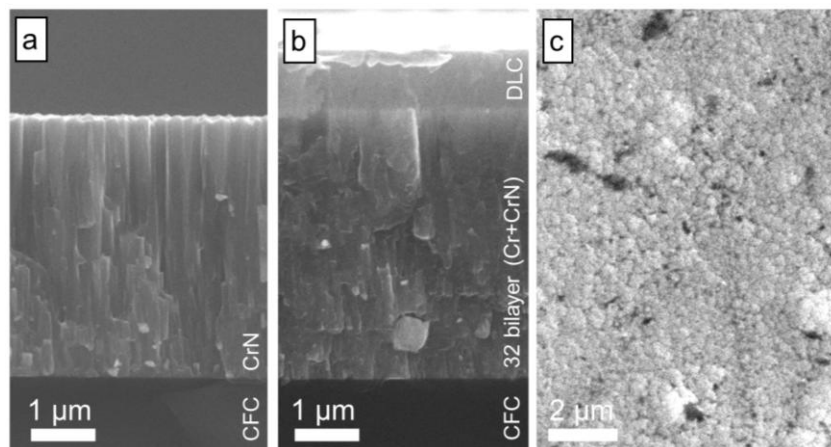
The dry friction at room temperature (21 °C) and at relative humidity of 50%–60% was evaluated on a ball-on-disc tribometer. 6 mm alumina (Al₂O₃) and hardened ferritic steel balls (AISI 5210, DIN ISO 100Cr6) were used as counterparts, sliding at wear tracks of 3.5 and 5 mm diameter, respectively. The applied load was 2 N, resulting in a maximum Hertzian contact pressure of 0.9 (Al₂O₃) and 0.8 GPa (AISI 5210). The sliding speed was set to 10 mm s⁻¹ and 10.000 laps (110 m and 157 m sliding distance, respectively) were tested. All these experiments were carried out on the as-deposited, clean surfaces. After testing, the wear tracks were inspected by optical light microscopy and profilometry to explain the wear mechanisms and analyze the wear profiles.

3. Results and Discussion

3.1. Film Topography and Microstructure

The microstructure and surface topography of the single layer CrN and multilayer Cr-CrN coatings on CFC substrates is shown in Figure 1. The CrN single layer coating in Figure 1a reveals a columnar structure of tapered crystals and fibrous grains in the cross-section, which is assigned to the “Zone 1” structure in the Thornton structure model [23]. This structure type is generally found for PVD coatings deposited at low temperatures and characterized by micro-cracks between the columns, pinholes, transient grain boundaries and through-coating porosity. This structure type merges at higher ion bombardment during deposition and thereby activated surface diffusion to a transition “Zone T” of fibrous grains with highly decreased porosity. Such refinement of grains is also visible for the multilayer Cr-CrN coating in Figure 1b, although the ion bombardment is rather similar to the CrN single layer coating. However, the necessary renucleation at the Cr-CrN and CrN-Cr layer boundaries in the multilayer coating during growth has similar effects on structural refinement: It decreases grain size and, thus, porosity at loosely bond cone boundaries. As expected, the DLC layer on the top (Figure 1b) is amorphous without distinct columnar growth features.

Figure 1. Growth structure and surface topography of magnetron sputtered coatings grown on fiber reinforced epoxy composites (CFC): Scanning electron microscopy (SEM) cross-sections of (a) ~4 μm CrN single layer coating and (b) ~4 μm 32 bilayer (Cr + CrN) coating with ~1 μm diamond-like carbon (DLC) top layer; (c) SEM top view of the coating from (b).



Compared to well-known coating topographies on polished steel substrates (e.g., shown in [24]) with fine spherical tops of the tapered crystallites, the topography of the coated CFC is much coarser and substantially different (Figure 1c): This is due to the about 30 times higher surface roughness of CFC compared to steel, which decisively influences the growth morphology (compare also to detailed descriptions in [10]) and reproduces the CFC substrate topography on the film surface. As visible with the decrease of Ra during the coating of CFC, the high roughness becomes smoother (Table 1), decreasing the roughness for the 32 (Cr-CrN) bilayer coating on CFC to a value, which is only 10 times that for the similar coating on polished austenitic steel.

Table 1. Arithmetic roughness (R_a) of uncoated substrates (carbon fiber reinforced epoxy composites (CFC), polished austenitic steel) and with deposited single layer and multilayer coatings.

Material/Coating	Roughness R_a [nm]	
	CFC	Steel
Uncoated substrate	75.2	2.4
CrN single layer	59.0	6.4
16 bilayers (Cr-CrN)	64.6	8.9
32 bilayers (Cr-CrN)	68.2	6.7
32 bilayers (Cr-CrN) + 1 μm DLC	109.3	15.1

TEM imaging of the growth structures of the Cr-CrN multilayers on steel substrates reveals important effects dependent on the thickness of the individual layers of the multilayers (Figure 2): The about 50% thicker Cr layer directly on the substrate surface shows much larger faceted, columnar and coarsened Cr grains than the second deposited thinner Cr layer after the first CrN layer (Figure 2a), which was afterwards repeatedly used in the multilayer stack. In addition, the density of formed microcracks in between the grains is higher for the thicker Cr layer. As visible in Figure 2b, no substantial coarsening in the subsequently deposited Cr-CrN multilayer occurs. The microcrack-like structures in the first Cr layer do not pass the interface to CrN and are only rarely found in the second Cr layer. Generally, the Cr grains were found to be larger (15–20 nm) than the CrN grains (5–10 nm size) (Figure 3a), although the Cr layers are thinner than the CrN layers (CrN/Cr ratio = 2:1). This seems to be due to the more complex fcc CrN structure (two overlapping NaCl lattices for Cr and for N) compared to single atom bcc Cr structure [25]. Crystallographic dependence is evident at the interface: The small mismatch of lattice constants of CrN ($a = 4.14 \text{ \AA}$) and Cr ($a = 4.588 \text{ \AA}$) allows stress compensation during nucleation by introduction of step dislocations (Figure 3c) in certain crystallographic orientations (e.g., (Cr (001) \parallel CrN (001) and Cr [100] \parallel CrN [110] [26]) (Figure 3b,d).

Figure 2. Transmission electron microscopy (TEM) cross-section images of a 32 bilayer (42 nm Cr + 84 nm CrN) coating on steel substrate: (a) multilayer film growth behavior close to the interface to the substrate; (b) growth close to the coating surface.

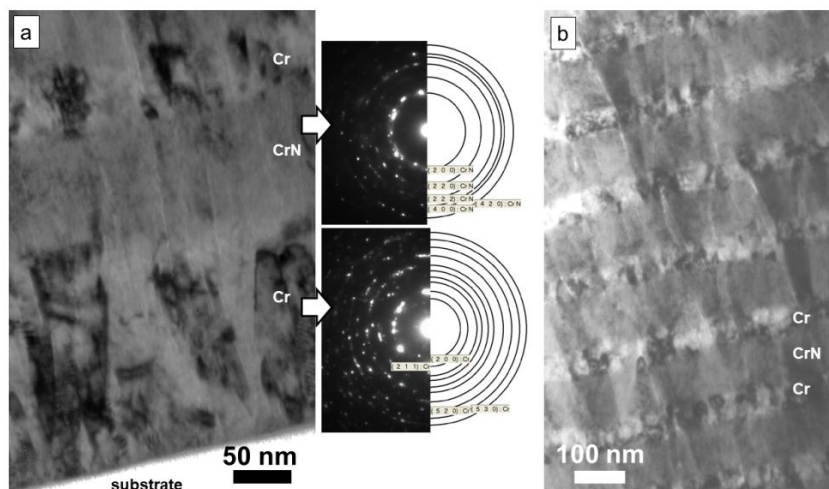
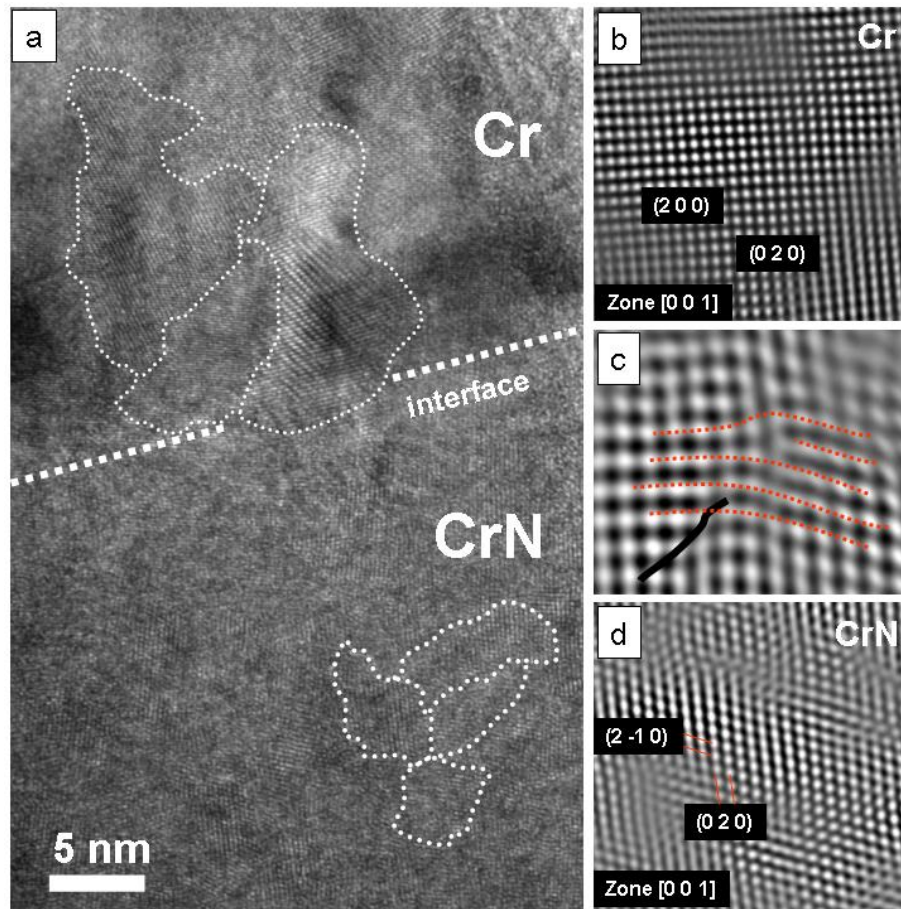
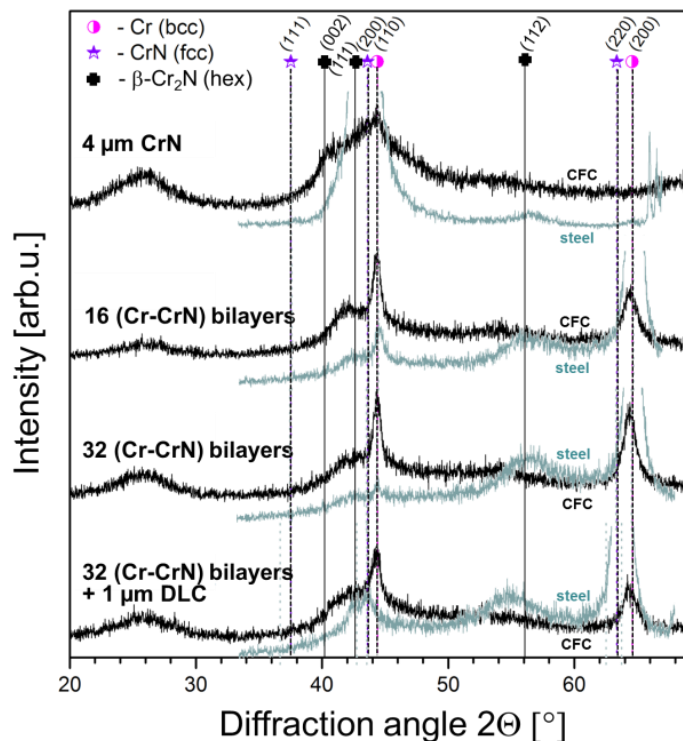


Figure 3. High resolution mode (HR)-TEM cross-section images of the interface growth mechanisms of a 32 bilayer (42 nm Cr + 84 nm CrN) coating on steel: (a) Overview indicating the grain structure and grain sizes; (b) Crystallographic analysis of the Cr layer; (c) Interface growth with dislocation formation; (d) Crystallographic analysis of the CrN layer.



The XRD phase analysis in Figure 4, comparing the coatings deposited on steel and CFC substrates, reveals high similarities in phases and orientations, although the substrate roughness is highly different: The Cr (200) peak of the coatings is more distinct on the steel than on the CFC substrate, which is connected to a higher phase content (higher crystallinity) and/or a larger Cr grain size. The peaks for all chromium nitride compounds (fcc CrN, hex β -Cr₂N [25]) are rather weak for the multilayer coatings, but they dominate the XRD spectra of the single layer with the (200) CrN peak. Only weak and broad (nanocrystalline to amorphous) diffraction is present for the β -Cr₂N phase: Nevertheless, it is stronger in (112) orientation for coated steel, but in (111) and (002) orientation for coated CFC substrates. The Cr (110) peak is only found for the films on CFC, but missing for films on steel, as also revealed by the diffraction pattern of the Cr interface layer in Figure 2a. The higher resolution in TEM diffraction patterns reveals further crystallographic phase features, not occurring in the XRD scans: strong (211) as well as weak (530) and (520) diffraction for Cr and weak (420) diffraction for CrN. The slight shift of the Cr (200) peak to lower diffraction angles could indicate tensile stresses in this phase.

Figure 4. Locked-couple X-ray diffraction scan of single CrN layer and (Cr + CrN) multilayer coatings on CFC (black spectra) and on steel (grey spectra) including assignment of peaks to standard peak positions from Powder Diffraction File (ICDD) (Cr (bcc): 00-027-1402, CrN (fcc): 03-065-2899, β -Cr₂N: 00-035-0803).



3.2. Mechanical Properties

The multi-layered structure directly influences the hardness and the elastic modulus of the coatings. Highest hardness on austenitic steel is evident for CrN single layer coatings (Table 2), while layering with Cr results in hardness decrease towards the Cr single layer hardness of around 12 GPa. Nevertheless, the hardness as a measure of the resistance against plastic deformation increases with the nanolayered structure with 32 bilayers of (42 nm Cr and 84 nm CrN) although the total metallic Cr weight content is similar to the 16 bilayer structure (84 nm Cr and 168 nm CrN). The elastic modulus (190–200 GPa) as well as the hardness values (15–16 GPa for the Cr-CrN multilayer coatings) are quite comparable to the literature (e.g., to the work of Romero *et al.* [27]), if a lateral contraction coefficient of 0.25–0.30 is assumed.

The described hardness behavior follows the Hall-Petch hardening relationship, which is theoretically based on the decrease in shearing capacity by dislocation pinning at the interfaces [26]. In contrast, the elastic modulus of these multilayers roughly follows the rule of mixture between Cr (~140 GPa) and CrN (~215 GPa) [28], being quite similar for both multilayer coatings with different bilayer modulation thickness. Adding the 1 μ m DLC top layer shifts hardness and elastic modulus towards the levels of single layer DLC films ($H \sim 14.5$ GPa, $E \sim 160$ GPa) due to the high enough load support for surface indentation and the low indentation depth (~0.35 μ m).

Table 2. Hardness and elastic modulus of single CrN layer and multilayer (Cr-CrN) coatings, determined on steel substrates.

Coating	Hardness [GPa]	Elastic modulus [GPa]
CrN single layer	17.8 ± 0.4	217 ± 4
16 bilayers (Cr-CrN)	15.0 ± 0.3	198 ± 4
32 bilayers (Cr-CrN)	16.0 ± 0.2	191 ± 3
32 bilayers (Cr-CrN) + 1 μm DLC	14.3 ± 0.3	156 ± 9

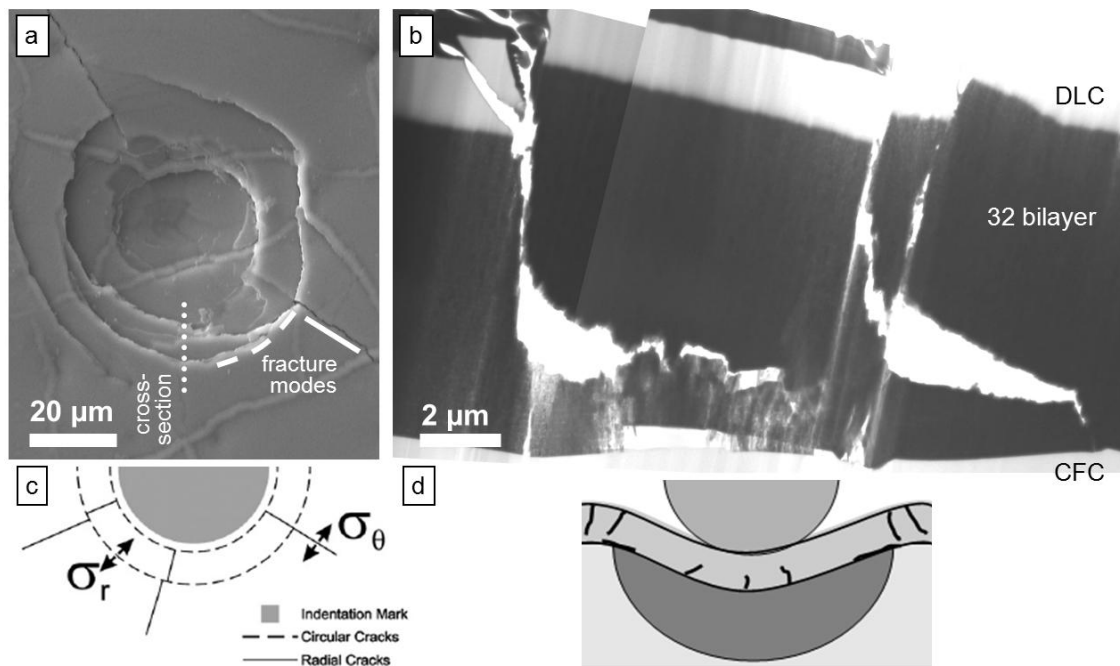
3.3. Deformation Mechanisms of the Coatings

The deformation mechanisms of coated CFC were studied by spherical indentation with high loads resulting in penetration depths of up to 7.5 μm. Such deep indents are necessary to trigger (visco-)elastoplastic flow of the epoxy matrix-rich CFC as well as deformation and fracture of the coating (top view in Figure 5a, cross-section in Figure 5b), if the yield or fracture strength is exceeded, respectively. Nevertheless, the influence of the deeper carbon fibers on surface deformation is only minor at these penetration depths in the epoxy layer.

FEM simulations of von-Mises stress distributions [7] reveal highest stressed regions below the indenter center at the coating-substrate interface, but also outside the contact, due to bending of the layer with maximum tensile stress at the coating surface. This is graphically shown in Figure 5c,d: The schematics in Figure 5d describes the loaded region in the cross-section, while the effect of elastoplastic flow of material below the indent outside the contact area, resulting in circular and radial cracks of the bulged region, is schematically shown in Figure 5c [29,30]: Ring cracks around the indent spread from the coating surface at the periphery of the contact and spread towards the substrate surface. Radial cracks in mild indentation with low local stress concentration (ball geometry, in contrast to pyramid-shaped indenters [30]) mainly occur, if alternative fracture mechanisms at lower stresses for energy dissipation are missing and the circumferential tensile stresses become too high. In the investigated series of single and multilayer coatings, such radial cracks are only observed for the 32 bilayer Cr-CrN systems, both with and without the DLC top layer. Such Cr-CrN load bearing layers possess the highest elasticity index (H/E ratio) and, thus, may also dissipate deformation energy elastically.

Ring crack formation is the main failure mechanism for all other films. Brittle crack propagation may occur at the columnar grain boundaries along existing microcracks (compare to Figure 2a) in the microstructure of the non-deformed materials due to the shear sliding of adjacent growth columns, which minimizes the shear loading [31]. The TEM cross-section image in Figure 5b shows the ring crack mode for a tough multilayer coating: Similar to preliminary investigations on the Ti-TiN multilayer coating system with soft Ti interlayers [19], the introduction of soft metal layers (Cr) in CrN for Cr-CrN multilayer structures fully changes the micromechanics of the films: While the single layered hard coatings (TiN, CrN) would fail by cohesive fracture through the whole coating thickness, such ring cracks in a multilayered film can be deflected and can change the propagation direction. The transition from tensile to shear fracture in the 32 Cr-CrN bilayer coating, is clearly visible in two instances in Figure 5b by the deflection of cracks from the direction normal to parallel to the substrate surface. After the deflection the crack propagation is arrested in the parallel shear crack.

Figure 5. (a) SEM top view of an indent by 2 N loading of a spherical indenter in 32 bilayer ($\text{Cr} + \text{CrN}$) and 1 μm DLC top layer coated CFC; (b) TEM cross-section prepared by Focussed Ion Beam (FIB) from the marked position in (a) indicating deformation and fracture; (c) Schematics of formation of circular/ring cracks (σ_r) and radial cracks (σ_θ); (d) Schematics showing plastically deformed region under a ball indent in a coated compound and localization of crack initiation/formation.

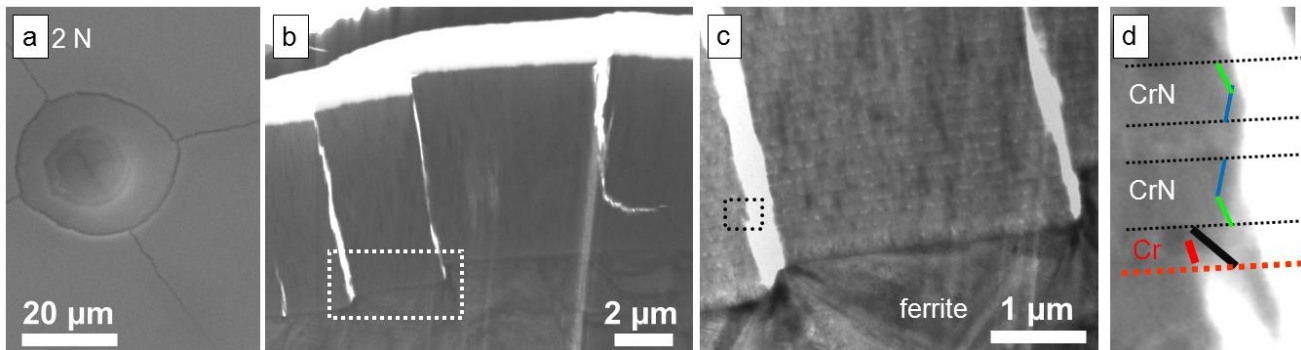


In load-depth curves obtained in instrumented indentation experiments, any coating fracture is observed as kink: Our experiments showed that first cohesive coating failure occurs for the 32 bilayer multilayer coating at ~1.2 μm penetration depth (~100 mN load). For the single layer CrN coating as well as for the 16 bilayer coating, kink formation is found at much lower loads (<60 mN) and at only 0.75 μm penetration depth. In comparison, first kink formation for the 32 bilayer coating on stiffer, less compliant austenitic steel substrates is found at ~850 mN load (~2.8 μm penetration depth).

The differences of indentation micromechanics for coatings on soft and hard substrates are very apparent from the above results for very soft epoxy CFC surfaces (E : 2–3 GPa, H < 0.1 GPa) (Figure 5) and stiffer substrate materials, e.g. austenitic steel (E : 210 GPa, H : 1.5 GPa) (Figure 6): Higher load support by the steel substrate decreases total deformation and, thus, the crack density of both radial and ring cracks on the surface (Figure 6a). Nevertheless, if the load bearing capacity of the coating is exceeded, fracture occurs and leads to localization of stresses on the substrate surface, which shear locally and introduces shear steps, which is well visible at the interface (Figure 6b). As revealed by the small crack on the very left side of Figure 6b, where crack propagation is stopped by the multi-layered architecture (interfaces), fracture in this investigated region starts from the interface. A distinct shear step is missing for this very small cracking event, because the stopped crack propagation prevented sliding of the crack flanks. Nevertheless, tensile stresses on the coating surface at higher distance to the indentation center also cause ring-like cracks after high substrate deformation (Figure 6a). These ring cracks are partly deflected to shear cracks (Figure 6b, on the very right). The detail at the crack flank in

Figure 6c and under high resolution in Figure 6d show in detail the mechanism of crack stopping in the multilayer: Shear deformation of the coating is concentrated in 45° planes of Cr layers, while the CrN layers show brittle fracture (fracture normal to the substrate surface).

Figure 6. Deformation behaviour of Cr-CrN multilayer coatings with 32 bilayers (CrN:Cr ratio = 2:1), deposited on austenitic steel and substrates. (a) Surface topography after indentation with 2 N load; (b) TEM cross-section of the deformed/fractured indent site; (c,d) Details of deformation and fracture as marked in (b) and (c).



Finally, the comparison of the micromechanical results with data obtained from scratch testing reveal for all coatings high adhesion on all substrate materials, while the cohesion of the coating is mainly dependent on the used layer architecture and the substrate type (mechanical behavior): Cohesive coating failure is present for the multilayer coated CFC at critical load $L_{c1} \sim 0.5$ N and for austenitic steel at ~ 1 N. Adhesive failure (L_{c2}) is missing for all systems even at maximum load of the scratch tester (30 N) and for ~ 50 μ m deformation depth.

3.4. Tribological Behavior of Coated CFC

Strains in tribological contacts are generally highly dynamical and fatigue plays an important role, even below the static yield strength. In coated systems, the compliance of the substrate decisively influences friction and wear, because bending both below and around the contact area introduces alternating tensile and compressive stresses in the substrate surface and coating. In the case of missing friction (friction coefficient $\mu = 0$), the maximum von-Mises stress is $\sim 35\%$ higher for the case of a stiff coating layer (E_1) on an elastic substrate ($E_2 = 1/2 E_1$) than in the non-coated case. However, friction plays a decisive role, affecting the tangential forces and, thus, the shear stresses in the coating-substrate system [31]. In the theory of pure indentation or at zero friction ($\mu = 0$), yielding in the coated surface always initiates at the coating/substrate interface below the center of the contact (highest von-Mises stresses), and the plastic zone does not grow towards the surface below the indenter [32,33]. Applying friction load ($\mu > 0$), the point of first yield moves from the center position backwards or forwards, depending on the friction coefficient [33]: For $\mu = 0.25$, the highest stressed region moves closer to the surface compared to the non-coated case, being $\sim 40\%$ higher as non-coated and $\sim 50\%$ as coated surface and $\mu = 0$. These values increase to $\sim 65\%$ and 125% for $\mu = 0.5$, respectively.

Based on these theoretical simulation model results it is clear, that the superposition of large elastic deformation of the coated elastic substrate from normal loading and the friction induced shear loads

easily leads to coating fracture and fatigue influenced phenomena like fragmentation and delamination, drastically influencing the tribological behavior.

Figures 7 and 8 show the evolution of friction coefficients in contact to Al_2O_3 and AISI 5210 steel counterpart balls in dependency of the contact lap number. For Al_2O_3 counterparts (Figure 7), the friction coefficient of all coatings is initially very low ($\mu \sim 0.08$). Ongoing sliding leads for the Cr-CrN multilayers to a sudden increase of friction up to 0.9, which slowly decreases to 0.6, which is the steady-state friction coefficient for uncoated CFC against Al_2O_3 . In contrast, the friction for the pure CrN coating as well as the multilayer with DLC top layer steadily increases from the initial level of 0.1–0.6, which is the value for uncoated CFC. The friction for the contact to AISI 5210 steel (Figure 8) is initially lower, but after the run-in generally higher for the CrN-based coatings without a DLC top layer ($\mu > 0.65$) than for the non-coated CFC substrate ($\mu \sim 0.5$). Only the multilayer composition with the DLC top layer enables a lower steady-state friction ($\mu \sim 0.17$) than is found for the non-coated contact, due to the well-known low friction coefficients of DLC-steel contacts.

A detailed analysis of the friction curves in Figures 7 and 8 in combination with an analysis of the wear tracks in Figures 9 and 10 is essential to understand the tribological mechanisms, which occur in sliding on the coated CFC surfaces: Based on friction stages proposed by Suh and Sin [34] the initial very low friction is mainly a result of ploughing the softer surface by asperities, starting for the investigated coatings on CFC with $\mu = 0.08$ and 0.045 for Al_2O_3 and steel counterparts, respectively. Based on the surface hardness, this ploughing mechanism by asperities occurs in contact to Al_2O_3 on the softer coating surface, but oppositely on the steel ball surface for this tribological contact. Although the mechanisms occurring in the initial friction contact were not investigated in this work, mechanisms occurring in later stages (mainly the transfer layer formation) indicate such behavior. Nevertheless, the high waviness and roughness of the coated CFC (see Table 1) enhances this low friction mechanism.

Repeated cyclic ploughing deformation quickly results in low-cycle fatigue fracture of asperities, leading to the next stage in the frictional contact. Both plastic deformation and fracture at high stresses contribute to smoothing and polishing the wear track, whereby wear debris is trapped in grooves. Additionally, cyclic deformation occurs inside and around the contact area due to the high compliance of the epoxy matrix of the substrate. Radial and ring cracks form during overloading, shown by the static indentation experiments above. These cohesive cracks and their propagation to adhesive cracks and coating delamination contribute additionally to the specific behavior of sliding on coated CFC surfaces.

As visible in Figures 7 and 8, the friction coefficient rapidly increases to >0.5 for the Cr-CrN multilayer coatings for both contact to Al_2O_3 and steel counterparts after the short run-in period, while friction coefficient for the CrN single layer hard coating in contact to Al_2O_3 as well as the coating types with DLC top layer are generally below the values for contact to uncoated CFC. The origin of this different behavior is the immediate formation of wear particles in sliding. Ploughing by wear particles results in high shear forces and, thus, high friction coefficients especially for coatings with the ability to shear like the multilayers with plastically deformable Cr layers. These particles are entrapped between the sliding surfaces and may form deformable and sticky transfer layers (tribolayers), which represent the steady-state condition of friction. The friction coefficients remain constant till the substrate is exposed e.g., by ploughing by the formed wear particles or delamination of the coating from the substrate surface whereby the coating finally failed.

Figure 7. Friction coefficients depending on the lap number (# contact cycles) for the tribological contact of an Al_2O_3 ball (6 mm) in ball-on-disk testing with uncoated and single and multilayer coated CFC under 2 N load and 3.5 mm wear track diameter (10,000 laps = 110 m sliding of pin).

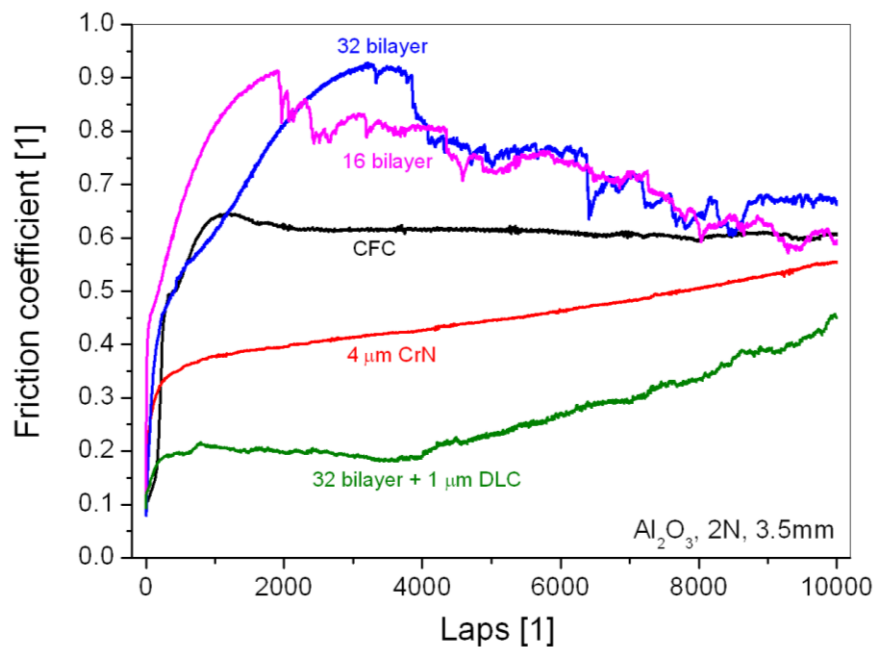


Figure 8. Friction coefficients depending on the lap number (# contact cycles) for the tribological contact of a DIN 100Cr6 / AISI 5210 steel ball (6 mm) in ball-on-disk testing with uncoated and single and multilayer coated CFC under 2 N load and 5 mm wear track diameter (10,000 laps = 157.1 m sliding of the pin).

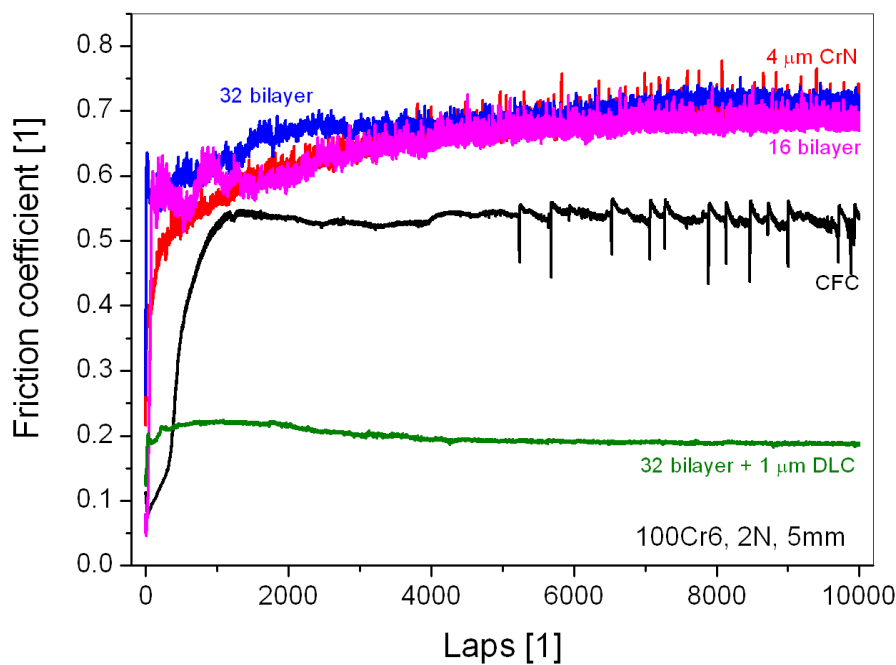
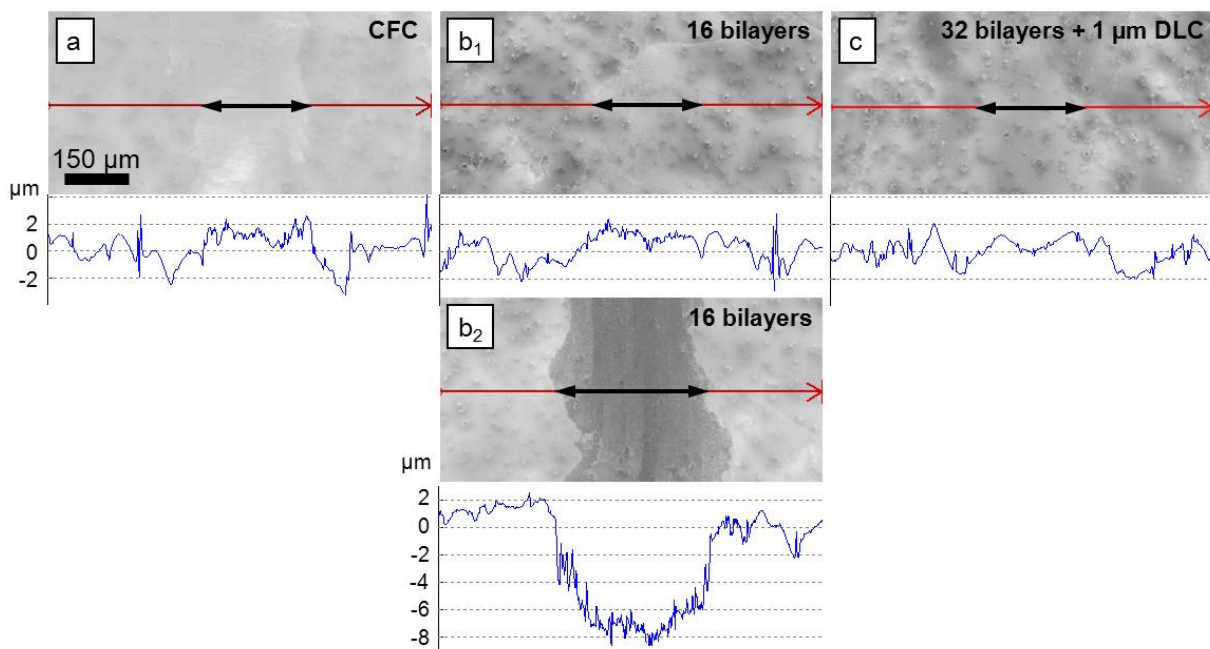


Figure 9. Light microscopy images and optical profilometry scans of the wear track after ball-on-disk testing with an Al_2O_3 ball (for experimental details see Figure 7) on (a) uncoated CFC; (b) CFC coated with 16 bilayers (Cr-CrN) (**b1**: undamaged coating with transfer layer, **b2**: highly abraded coating and substrate, both found on the same wear track); and (c) CFC coated with 32 bilayers (Cr + CrN) and 1 μm DLC top layer. The long arrows indicate the profilometry scan lines, the short bold arrows the approximate width of the wear tracks.



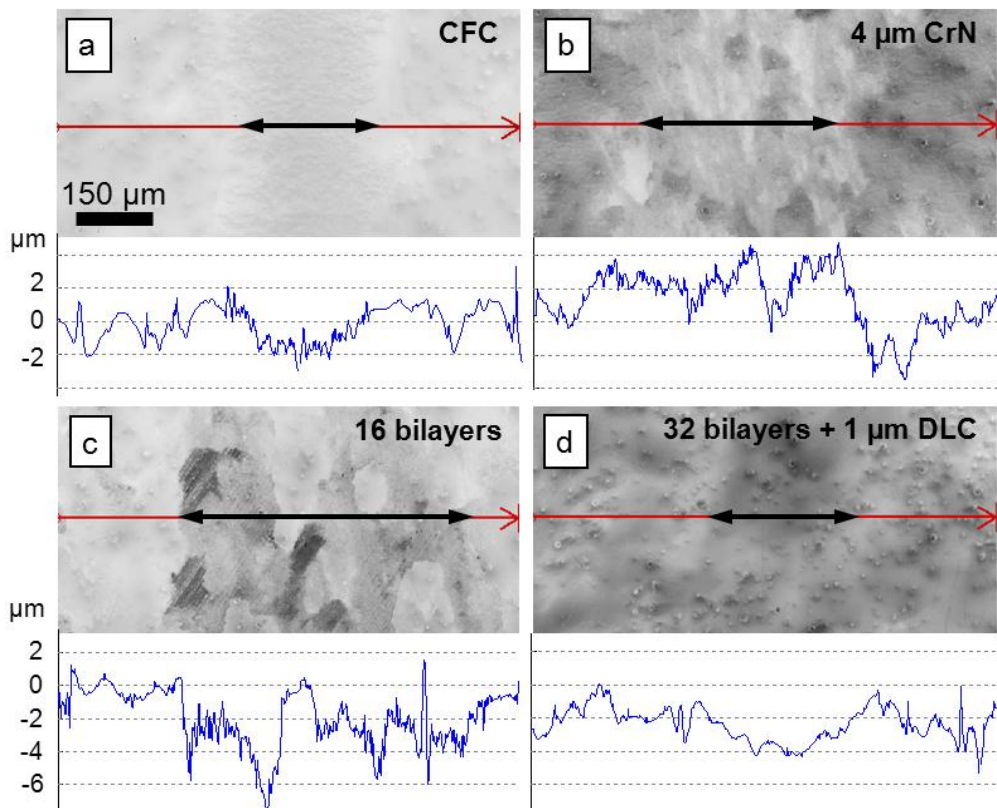
Cr-CrN multilayer coating contacts to Al_2O_3 counterparts show very high friction coefficients of up to 0.94 in this steady-state regime (Figure 7). However, the shearing of metal Cr under cyclic loading, fatigue fracture, the formation of abrasive wear debris and transfer layer adhesion on the Al_2O_3 counterpart due to sticky wear debris results in quick partial failure of the coating (Figure 9b), baring the substrate surface. Transfer of epoxy polymer from these areas forms polymeric transfer layers (based on SEM EDS analysis) at the whole wear scar on ball and disc, which decreases the friction significantly. During sliding, frictional heat may chemically modify the bared polymer and the polymer transfer layers (introduction of atoms from ambient atmosphere, cross-linking and polymer chain scissoring, *etc.* [35]). The formation of a thick tribolayer (transfer layer) on the uncoated CFC indicates such a mechanism as the main contribution in the tribological behavior for contact to Al_2O_3 (Figure 9a). The repeated sudden changes of the friction coefficient during on-going sliding for the Cr-CrN multilayer coatings (Figure 7) indicate furthermore stepwise delamination and new formation of transfer layers.

The single layer CrN behaves differently in tribological contact to Al_2O_3 due to lack of shearing at softer Cr layers and lower adhesion of transfer layers of the worn coating on the counterpart. Furthermore, cracking in the coating around the contact area runs generally through the whole film thickness during overloading, whereby large coating fragments delaminate. This process starts very early after the run-in period, which is visible by a partly bared CFC substrate surface in the wear track. Missing adhesion of transfer layers on the Al_2O_3 keep the friction coefficient low. Nevertheless, ongoing grinding wear of CrN wear debris increases bared CFC substrate surfaces in the wear track and increases

the friction coefficient towards the value measured for sliding of Al_2O_3 on uncoated CFC (Figure 7). Finally, wear of the partly bared substrate surface contributes to a transfer layer formation on both the CrN as well as on the counterpart.

In sliding of AISI 5210 counterparts on CrN and Cr-CrN coatings, a thick transfer layer is generally formed in the steady-state stage by mechanical mixing on the top of the CrN surface (Figure 10b,c). Based on SEM EDS analysis, this transfer layer consists of Fe, Cr, N, O and hydrocarbons. Its formation is mainly due to asperity fatigue mechanisms, in which the harder coating wears the softer steel counterpart. Nevertheless, the asperity fracture and coating delamination/spallation mechanisms do not stop after formation of the transfer layer, which is visible in the deep grooves down into the CFC substrate in the depth profile of the 16 bilayer coating (Figure 10b). In comparison, wear of uncoated CFC is mainly due to grinding by asperities of the much harder steel ball (Figure 10a).

Figure 10. Light microscopy images and optical profilometry scans of the wear track after ball-on-disk testing with a DIN 100Cr6 / AISI 5210 steel ball (for experimental details see Figure 8) on (a) uncoated CFC; (b) CFC coated with $\sim 4 \mu\text{m}$ CrN single layer coating; (c) CFC coated with $\sim 4 \mu\text{m}$ 16 bilayer Cr-CrN multilayer coating; and (d) CFC coated with 32 (Cr + CrN) bilayers and a 1 μm DLC top layer. The long arrows indicate the profilometry scan lines, the short bold arrows the approximate width of the wear tracks.



Main tribological improvements can be achieved by low-friction DLC top layer both for the sliding of AISI 5210 steel and Al_2O_3 balls. The coated structure is not substantially damaged during the investigated sliding distance in all cases (Figures 9c and 10d). This superior behavior is mainly due to the low friction coefficients and the decreased tribological stresses (low shearing component).

4. Conclusions

CrN single layer and Cr-CrN multilayer coatings of ~4 μm thickness, partly finished with a 1 μm DLC top layer, were deposited by magnetron sputtering at low temperatures on soft carbon-fiber strengthened composite substrates in order to increase their tribological resistance in sliding applications. All multilayer coatings possess a very fine grained, columnar microstructure and have much less severe intercolumnar microcracks than the CrN single layer coating. The coatings on CFC have dome-shaped topography and reproduce the high CFC substrate roughness. The elastic modulus decreases for the Cr-CrN multilayer coatings by the introduction of the softer Cr layers compared to CrN single layer coatings following the rule of mixture. In contrast, the hardness of the multilayers is only slightly decreased compared to CrN by the softer Cr phase.

The growth structure has significant influence on the deformation properties: The higher the tendency to crack deflection in the multilayer by the higher density of interfaces, the more pronounced is the formation of radial cracks in the surrounding of static ball indentation, as well as the crack deflection to shear cracks. However, no significant improvements by CrN single layer and Cr-CrN multilayer coatings were achieved in tribological ball-on-disc testing compared to uncoated CFC due to high friction coefficients ($\mu > 0.6$) in contact to AISI 52100 steel and Al_2O_3 counterparts. Only the application of amorphous DLC top layers significantly decreases friction coefficients to ~0.2, which drastically lowers the tangential shear forces in the coating. Minimized wear of these DLC top layers on the tough Cr-CrN multilayer films resulted in survival of these coating in tribology testing (10^4 cycles under 2 N loading) with capacity to much higher sliding cycles with low-friction behavior.

Acknowledgments

The financial support of this work by the Austrian Federal Ministry of Traffic, Innovation and Technology, Austrian within the frame of the Austrian Nanoinitiative programme and the MNT-ERA.NET programme with additional support of the European Union and the Federal Country of Styria (Austria), the Polish-Austrian exchange project PL 12/2010 (funded in Austria by the Oesterreichischer Austauschdienst OeAD), and the research project of the Polish National Science Centre No. 3066/B/T02/2011/40 is highly acknowledged. The authors want to thank Harald Parizek from JOANNEUM RESEARCH for coating deposition as well as Christian Mitterer's research group at the University of Leoben for XRD analysis.

Conflicts of Interest

The authors declare no conflict of interest.

References

1. Ivosevic, M.; Knight, R.; Kalidindi, S.R.; Palmese, G.R.; Sutter, J.K. Adhesive/cohesive properties of thermally sprayed functionally graded coatings for polymer matrix composites. *J. Therm. Spray Technol.* **2005**, *14*, 45–51.
2. Palumbo, G.; Brooks, I.; Panagiotopoulos, K.; McCrea, J.; Limoges, D.; Erb, U. Strong lightweight article containing a fine-grained metallic layer. U.S. Patent 7,387,578 B2, June 2008.

3. Friedrich, C.; Gadow, R.; Speicher, M. Protective multilayer coatings for carbon–carbon composites. *Surf. Coat. Technol.* **2002**, *151*, 405–411.
4. He, M.Y.; Evans, A.G.; Hutchinson, J.W. Crack deflection at an interface between dissimilar elastic materials: role of residual stresses. *Int. J. Solids Struct.* **1994**, *31*, 3443–3455.
5. Biron, M. *Thermosets and Composites*; Elsevier: Oxford, UK, 2004.
6. Zhang, S.; Sun, D.; Fu, Y.; Du, H. Toughening of hard nanostructural thin films: A critical review. *Surf. Coat. Technol.* **2005**, *198*, 2–8.
7. Karimi, A.; Wang, Y.; Cselle, T.; Morstein, M. Fracture mechanisms in nanoscale layered hard thin films. *Thin Solid Films* **2002**, *420*, 275–280.
8. Chen, Z.; Cotterell, B.; Wang, W. The fracture of brittle thin films on compliant substrates in flexible displays. *Eng. Fract. Mech.* **2002**, *69*, 597–603.
9. Kääriänen, T.; Rahamathunnisa, M.; Tanttari, M.; Cameron, D.C. Properties of Magnetron Sputtered Hard Coatings on Carbon and Glass Fibre Composites. In Proceedings of 49th Annual Technical Conference, Washington, DC, USA, 22–27 April 2006; pp. 548–554.
10. Lackner, J.M.; Waldhauser, W.; Ganser, C.; Teichert, C.; Kot, M.; Major, L. Mechanisms of topography formation of magnetron-sputtered chromium-based coatings on epoxy polymer composites. *Surf. Coat. Technol.* **2013**, in press.
11. Voevodin, A.A.; Schneider, J.M.; Rebholz, C.; Matthews, A.. Multilayer composite ceramicmetal-DLC coatings for sliding wear applications. *Tribol. Int.* **1996**, *29*, 559–570.
12. Stueber, M.; Holleck, H.; Leiste, H.; Seemann, K.; Ulrich, S.; Ziebert, C. Concepts for the design of advanced nanoscale PVD multilayer protective thin films. *J. Alloys Compd.* **2009**, *483*, 321–333.
13. Chan, K.S.; He, M.Y.; Hutchinson, J.W. Cracking and stress redistribution in ceramic layered composites. *Mater. Sci. Eng. A* **1993**, *167*, 57–64.
14. Leyland, A.; Matthews, A. Thick Ti/TiN multilayered coatings for abrasive and erosive wear resistance. *Surf. Coat. Technol.* **1994**, *70*, 19–25.
15. Holmberg, K.; Matthews, A.; Ronkainen, H. Coatings tribology—Contact mechanisms and surface design. *Tribol. Int.* **1998**, *31*, 107–120.
16. Martinez, E.; Romero, J.; Lousa, A.; Esteve, J. Nanoindentation stress–strain curves as a method for thin-film complete mechanical characterization: application to nanometric CrN/Cr multilayer coatings. *Appl. Phys. A* **2003**, *77*, 419–427.
17. Smolik, J.; Zdunek, K.; Larisch, B. Investigation of adhesion between component layers of a multi-layer coating TiC/Ti (CxN_{1-x})/TiN by the scratch-test method. *Vacuum* **1999**, *55*, 45–50.
18. Lackner, J.M.; Waldhauser, W.; Schwarz, M.; Mahoney, L.; Major, L.; Major, B. Polymer pre-treatment by linear anode layer source plasma for adhesion improvement of sputtered TiN coatings. *Vacuum* **2008**, *83*, 302–307.
19. Kot, M.; Rakowski, W.; Major, Ł.; Lackner, J.M. Load-bearing capacity of coating-substrate systems obtained from spherical indentation tests. *Mater. Des.* **2012**, *43*, 99–111.
20. Lackner, J.M.; Major, L.; Kot, M. Microscale interpretation of tribological phenomena in Ti/TiN soft-hard multilayer coatings on soft austenite steel substrates. *Bull. Pol. Acad. Sci. Tech. Sci.* **2011**, *59*, 343–355.

21. DIN EN ISO 14577-1:2002 Metallic Materials—Instrumented Indentation Test for Hardness and Materials Parameters. Part 1: Test Method; International Organization for Standardization: Geneva, Switzerland, 2002.
22. Oliver, W.C.; Pharr, G.M. Improved technique for determining hardness and elastic modulus using load and displacement sensing indentation experiments. *J. Mater. Res.* **1992**, *7*, 1564–1583.
23. Thornton, J.A. Influence of apparatus geometry and deposition conditions on the structure and topography of thick sputtered coatings. *J. Vac. Sci. Technol.* **1974**, *11*, 666–670.
24. Jung, M.J.; Nam, K.H.; Jung, Y.M.; Han, J.G. Nucleation and growth behavior of chromium nitride film deposited on various substrates by magnetron sputtering. *Surf. Coat. Technol.* **2002**, *171*, 59–64.
25. JCPDS-International Centre for Diffraction Data. Cards No. 00-027-1402 (Si), 00-035-0803 (-Cr₂N), 03-06899 (CrN), 00-027-1402 (Cr).
26. Hall, E.O. The deformation and ageing of mild steel: III discussion of results. *Proc. Phys. Soc. B* **1951**, *64*, doi:10.1088/0370-1301/64/9/303.
27. Romero, J.; Esteve, J.; Lousa, A. Period dependence of hardness and microstructure on nanometric Cr/CrN multilayers. *Surf. Coat. Technol.* **2004**, *188*, 338–343.
28. Chen, H.Y.; Tsai, C.J.; Lu, F.H. The Young's modulus of chromium nitride films. *Surf. Coat. Technol.* **2004**, *184*, 69–73.
29. Hutchinson, J.W.; Thouless, M.D.; Liniger, E.G. Growth and configurational stability of circular, buckling-driven film delaminations. *Acta Metall. Mater.* **1992**, *40*, 295–308.
30. Tabor, D. Indentation Hardness and Its Measurement: Some Cautionary Comments. In *Microindentation Techniques in Material Science and Engineering*; Blau, P.J., Lawn, B.R., Eds.; American Society of Testing of Materials: Ann Arbor, MI, USA, 1986; p. 129.
31. Holmberg, K.; Matthews, A. *Coatings Tribology, Properties, Techniques and Applications in Surface Engineering*; Elsevier: Amsterdam, The Netherlands, 1996.
32. Komvopoulos, K. Elastic-plastic finite element analysis of indented layered media. *Trans. ASME J. Tribol.* **1989**, *111*, 430–439.
33. O'Sullivan, T.C.; King, R.B. Sliding contact stress field due to a spherical indenter on a layered elastic half-space. *J. Tribol.* **1998**, *110*, 235–240.
34. Suh, N.P.; Sin, H.C. The genesis of friction. *Wear* **1981**, *69*, 91–114.
35. Stachowiak, G. *Wear: Materials, Mechanisms and Practice*; Wiley: Chichester, UK, 2005.

© 2014 by the authors; licensee MDPI, Basel, Switzerland. This article is an open access article distributed under the terms and conditions of the Creative Commons Attribution license (<http://creativecommons.org/licenses/by/3.0/>).